ADVANCES IN ATMOSPHERIC SCIENCES, VOL. 31, NOVEMBER 2014, 1267–1278

Effect of Baroclinicity on Vortex Axisymmetrization. Part II: Baroclinic Basic Vortex

Jiayi PENG*[1], Melinda S. PENG[2], Tim LI[3], and Eric HENDRICKS[2]

[1]*IMSG at Environmental Modeling Center, NCEP/NOAA, College Park, Maryland, USA*
[2]*Naval Research Laboratory, Monterey, California, USA*
[3]*Department of Meteorology and IPRC, University of Hawaii at Manoa, Honolulu, Hawaii, USA*

(Received 15 December 2013; revised 1 March 2014; accepted 31 March 2014)

ABSTRACT

The effect of baroclinicity on vortex axisymmetrization is examined within a two-layer dynamical model. Three basic state vortices are constructed with varying degrees of baroclinicity: (i) barotropic, (ii) weak baroclinic, and (iii) strong baroclinic. The linear and nonlinear evolution of wavenumber-2 baroclinic disturbances are examined in each of the three basic state vortices. The results show that the radial propagating speed of the vortex Rossby wave at the lower level is larger with the stronger baroclinicity, resulting in a faster linear axisymmetrization process in the stronger baroclinic vortex.

It is found that the nonlinear axisymmetrization process takes the longest time in the strongest baroclinic vortex among the three different basic vortices due to the weaker kinetic energy transfer from asymmetric to symmetric circulations at the lower level. A major finding in this study is that the same initial asymmetric perturbation can have different effects on symmetric vortices depending on the initial vortex baroclinicity. In numerical weather prediction models, this implies that there exists a sensitivity of the subsequent structural and intensity change solely due to the specification of the initial vertical shear of the tropical cyclone vortex.

Key words: vortex axisymmetrization, asymmetry, baroclinicity

Citation: Peng, J., M. S. Peng, T. Li, and E. Hendricks, 2014: Effect of baroclinicity on vortex axisymmetrization. Part II: Baroclinic basic vortex. *Adv. Atmos. Sci.*, **31**(6), 1267–1278, doi: 10.1007/s00376-014-3238-9.

1. Introduction

Asymmetric perturbations such as convection near the inner core of a tropical cyclone will be tilted by the basic shear flows, such that the perturbation energy will be converted to the symmetric mean flows which will strength the parent vortex. This is the vortex axisymmetrization process, which is closely related to tropical cyclone structure and intensity change (Carr and Williams, 1989; Smith and Montgomery, 1995; Montgomery and Enagonio, 1998; Möller and Montgomery, 1999, 2000; Shapiro, 2000; Enagonio and Montgomery, 2001; Wang, 2002).

To investigate spiral bands in a hurricane, Montgomery and Kallenbanch (1997) described the vortex axisymmetrization process through the vortex Rossby wave propagation. Peng et al. (2008) constructed a barotropic dynamic model to examine the vortex axisymmetrization process. The characteristics of the initial asymmetric perturbations, including their different positions, azimuthal and radial profiles, could have significant effects on vortex axisymmetrization.

In Part I of this two-part paper (Peng et al., 2014), the barotropic and baroclinic disturbances axisymmetrized by the barotropic basic vortex are investigated in a two-layer dynamic model. The results show that the radial propagation of a baroclinic disturbance is slower than a barotropic disturbance, resulting in a slower linear axisymmetrization for baroclinic disturbances. The slower-propagating baroclinic waves induce more baroclinic asymmetric kinetic energy (KE) to be transferred to the barotropic symmetric vortex than from barotropic waves, resulting in a faster axisymmetrization process in the nonlinear baroclinic wave experiment than in the nonlinear barotropic wave experiment.

In this, Part II of the paper, we focus on the baroclinic vortex Rossby wave propagation under the environmental flows of the baroclinic vortex, as well as their nonlinear interactions and energy exchanges. As described in Part 1 (Peng et al., 2014), a barotropic vortex, denoted as TC1, has $R_{\max} = 0.1$ (100 km) and $V_{\max} = 0.5$ (25 m s^{-1}) at both the upper and lower levels. A strong baroclinic vortex applied here, in Part 2, denoted as TC2, has a maximum tangential wind of $V_{\max} = 0.5$ (25 m s^{-1}) at the lower level and $V_{\max} = -0.5$ (anticyclonic flow) at the upper level. A weak baroclinic vortex, denoted as TC3, has a strong cyclone ($V_{\max} = 0.5$) at the lower level and a weak cyclone ($V_{\max} = 0.25$) at the upper level (Peng et al., 2014, Fig. 1). The same baroclinic

* Corresponding author: Jiayi PENG
Email: jiayi.peng@noaa.gov

disturbances as in experiment LBC in Peng et al. (2014) is used in all experiments of this paper. The linear experiment WLBC has a weak baroclinic basic vortex (TC3), and experiment SLBC has a strong baroclinic basic vortex (TC2). Their corresponding nonlinear experiments are denoted as WNBC and SNBC, respectively. A detailed description of these experiments is given Peng et al. (2014, Table 1).

The structure of this paper is as follows. The baroclinic asymmetric perturbations axisymmetrized by the vortices with different baroclinicity is discussed in section 2. Section 3 investigates the energy conversion among the barotropic (baroclinic) symmetric flows and barotropic (baroclinic) asymmetric perturbations. A summary and discussion are provided in section 4.

2. Axisymmetrization with different baroclinic vortices

Observations indicate that both the symmetric and asymmetric components of tropical cyclones have strong baroclinic structure (Marks and Houze, 1987; Reasor et al., 2000; Rogers et al., 2012). In this section, we investigate how an initially baroclinic perturbation is axisymmetrized by a baroclinic basic vortex. Two basic baroclinic vortices are designed, including a weak baroclinic vortex (TC3) and a strong baroclinic basic vortex (TC2). The initial asymmetry is baroclinic, as in the LBC and NBC cases (Peng et al., 2014, Table 1). Note that the initial circulations at the lower level have the same structure as the barotropic vortex (experiments LBC/NBC). Therefore, the analyses for the experiments in this study are focused on their lower-level components.

2.1. *Linear simulations*

The evolution of the asymmetric vorticity in the linear cases WLBC and SLBC and their departures from LBC are depicted in Fig. 1. The initial baroclinic asymmetric disturbance in both the weak and strong baroclinic vortex induces stronger inner-core asymmetry, and the stronger baroclinic vortex has even larger inner asymmetry (Fig. 1). The negative difference region near and outside the radius of maximum wind (RMW) (Figs. 1c and d) indicates that the initial baroclinic asymmetric disturbance will be axisymmetrized faster in the stronger baroclinic symmetric vortex. The radial propagating speed of the vortex Rossby wave at the lower level is faster with the stronger baroclinicity, resulting in a faster axisymmetrization process in the stronger baroclinic vortex (figure not shown).

The linear vorticity equation for the lower level, given in the following, is used to examine different evolutions of the

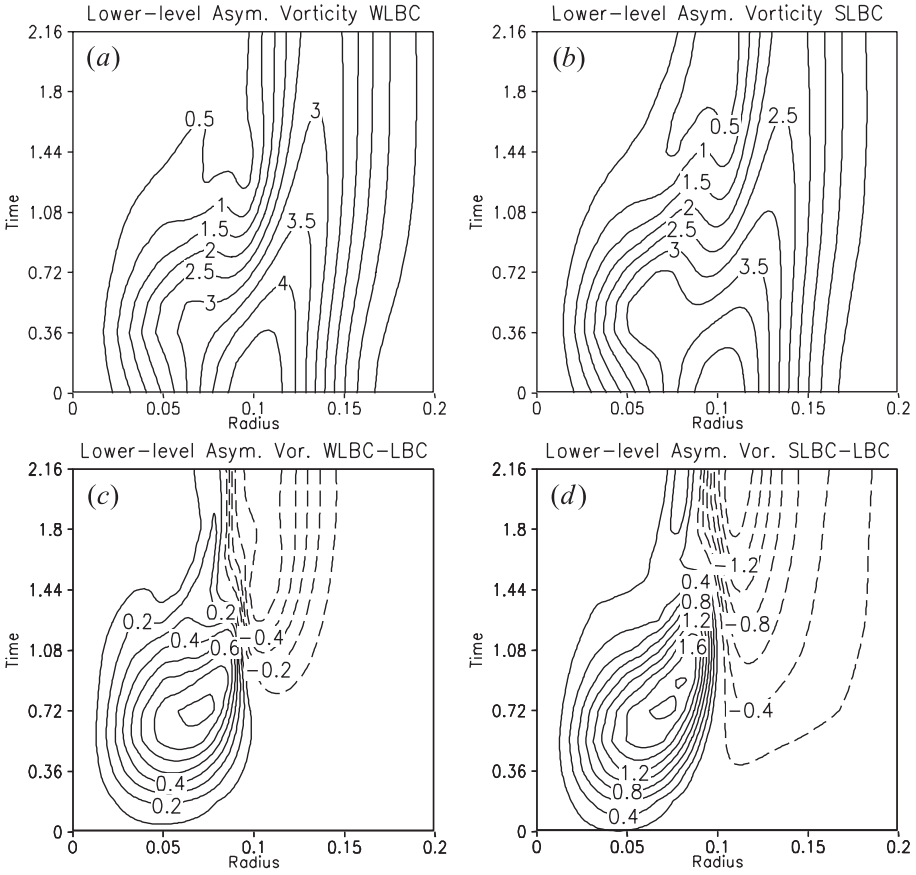

Fig. 1. The time–radius cross section of the asymmetric vorticity amplitude at the lower level in case (a) WLBC, (b) SLBC, and (c, d) their differences from LBC, respectively.

asymmetric disturbances in different symmetric vortices.

$$\frac{\partial \zeta_3'}{\partial t} = -\left(\bar{u}_3\frac{\partial \zeta_3'}{\partial x} + \bar{v}_3\frac{\partial \zeta_3'}{\partial y}\right) - \left(u_3'\frac{\partial \bar{\zeta}_3}{\partial x} + v_3'\frac{\partial \bar{\zeta}_3}{\partial y}\right) - (1+\bar{\zeta}_3)\left(\frac{\partial u_3'}{\partial x} + \frac{\partial v_3'}{\partial y}\right), \quad (1a)$$

$$\frac{\partial \zeta_3'}{\partial t} = -\left(\bar{u}_3\frac{\partial \zeta_3'}{\partial x} + \bar{v}_3\frac{\partial \zeta_3'}{\partial y}\right) - \left(u_3'\frac{\partial \bar{\zeta}_3}{\partial x} + v_3'\frac{\partial \bar{\zeta}_3}{\partial y}\right) - \left[\left(1+\frac{5}{4}\bar{\zeta}_3\right)\left(\frac{\partial u_3'}{\partial x}+\frac{\partial v_3'}{\partial y}\right)+\frac{1}{4}\bar{v}_3\frac{\partial}{\partial x}\left(\frac{\partial u_3'}{\partial x}+\frac{\partial v_3'}{\partial y}\right)-\frac{1}{4}\bar{u}_3\frac{\partial}{\partial y}\left(\frac{\partial u_3'}{\partial x}+\frac{\partial v_3'}{\partial y}\right)\right], \quad (1b)$$

$$\frac{\partial \zeta_3'}{\partial t} = -\left(\bar{u}_3\frac{\partial \zeta_3'}{\partial x} + \bar{v}_3\frac{\partial \zeta_3'}{\partial y}\right) - \left(u_3'\frac{\partial \bar{\zeta}_3}{\partial x} + v_3'\frac{\partial \bar{\zeta}_3}{\partial y}\right) - \left[(1+2\bar{\zeta}_3)\left(\frac{\partial u_3'}{\partial x}+\frac{\partial v_3'}{\partial y}\right)+\bar{v}_3\frac{\partial}{\partial x}\left(\frac{\partial u_3'}{\partial x}+\frac{\partial v_3'}{\partial y}\right)-\bar{u}_3\frac{\partial}{\partial y}\left(\frac{\partial u_3'}{\partial x}+\frac{\partial v_3'}{\partial y}\right)\right], \quad (1c)$$

where Eqs.(1a),(1b) and (1c) represent the evolution of asymmetric vorticity at the lower level in case LBC, WLBC and SLBC, respectively, with ζ_3' representing the asymmetric perturbation vorticity and $\bar{\zeta}_3$ the symmetric vorticity at the lower level. The first term on the right-hand side of Eqs. (1a) to (1c) represents the perturbation vorticity advection by the mean flows at the lower level; the second term represents the basic vorticity advection by perturbation flows; and the third term represents the vorticity change by lower-level divergence.

The first two terms on the right-hand side of Eqs. (1a) to (1c) are the same. The difference comes from the third term, the divergence term. For the LBC case (the initial baroclinic disturbance in a barotropic vortex, TC1), Eq. (1a) could be derived from Eq. (6) in Peng et al. (2014) by using $\zeta_3' = -\zeta_d'$, $u_3' = -u_d'$, $v_3' = -v_d'$, $\bar{\zeta}_3 = \bar{\zeta}_a$, $\bar{u}_3 = \bar{u}_a$, and $\bar{v}_3 = \bar{v}_a$. Therefore, the relationship between the baroclinic asymmetric vorticity and the divergence in Eq. (6) of Peng et al. (2014) is the same as that in Eq. (1a) for the lower-level asymmetric vorticity and divergence. As illustrated in Peng et al. (2014), the initial baroclinic asymmetry could generate new lower-level asymmetry inside the RMW in the early stage. The divergence term always has a negative effect on the inner core asymmetric vorticity at the lower level (see Peng et al., 2014, Fig. 5). In contrast, the positive effect by the divergence term is imposed on the outer original asymmetric vorticity. Furthermore, the OMEGA equation diagnosis shows that the warm (cold) advection by the symmetric mean flow in case LBC induces the phase difference between the asymmetric divergence and vorticity at the lower level, as shown in Peng et al. (2014, Fig. 6).

For the WLBC case (an initial baroclinic disturbance with

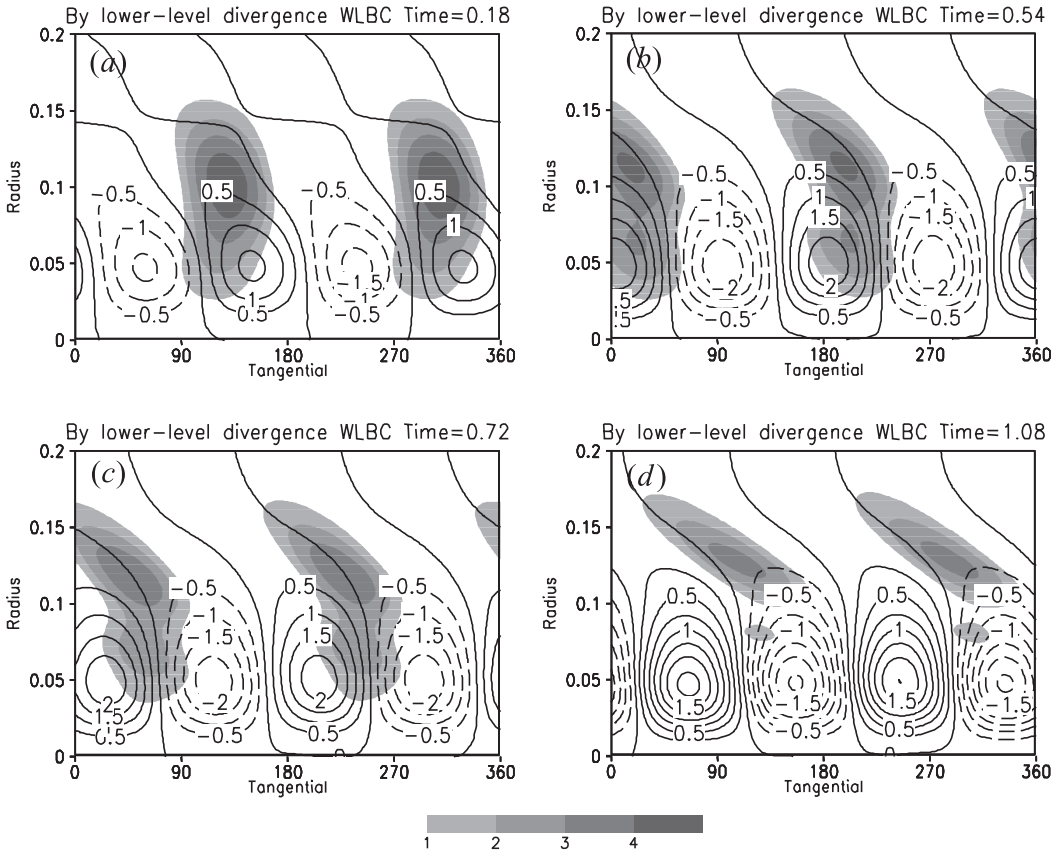

Fig. 2. The lower-level vorticity changed by divergence in case WLBC at time (a) 0.18, (b) 0.54, (c) 0.72, and (d) 1.08. Shading represents the positive asymmetric vorticity.

a weak baroclinic vortex, TC3), the initial baroclinic perturbations will generate the lower-level asymmetric vorticity inside the RMW in the early stage, as in LBC. The divergence term has a positive effect on the lower-level asymmetric vorticity near and inside the outer cell in the early stage before time 0.72 (Figs. 2a–c), so the asymmetry is larger than the LBC asymmetry inside the RMW (Fig. 1c). Since the divergence term propagates slower than the vorticity field in the azimuthal direction, its positive region begins to lag the positive vorticity region and has a negative effect after time 0.72 (Fig. 2d). In comparison, the divergence term remains locked in phase with the asymmetric vorticity in LBC. This causes a faster decaying of the asymmetry in WLBC than in LBC.

The diagnosis of Eq. (7) in Peng et al. (2014) (the OMEGA equation) is examined to understand the relation between the asymmetric vorticity and divergence at lower level. The left-hand side of Eq. (7) in Peng et al. (2014) can be related to the divergence at the lower level, i.e., $\nabla^2(-\omega_2/\Delta p) - (1+\zeta_a)(-\omega_2/\Delta p) \propto \delta_3$. Overall, the fifth and sixth terms make the largest contribution to the evolution of the lower-level asymmetric divergence in terms of $\delta_3 \propto \overline{\boldsymbol{V}}_a \cdot \nabla T' + \boldsymbol{V}'_a \cdot \nabla \overline{T}$. The evolution of the fifth term, the sixth term, and the sum of all the terms on the right-hand side of Eq. (7) in Peng et al. (2014) are depicted in Fig. 3. The warm advection by the barotropic mean flows ($-\overline{\boldsymbol{V}}_a \cdot \nabla T' > 0$) and the barotropic perturbation flow ($-\boldsymbol{V}'_a \cdot \nabla \overline{T} > 0$) located near

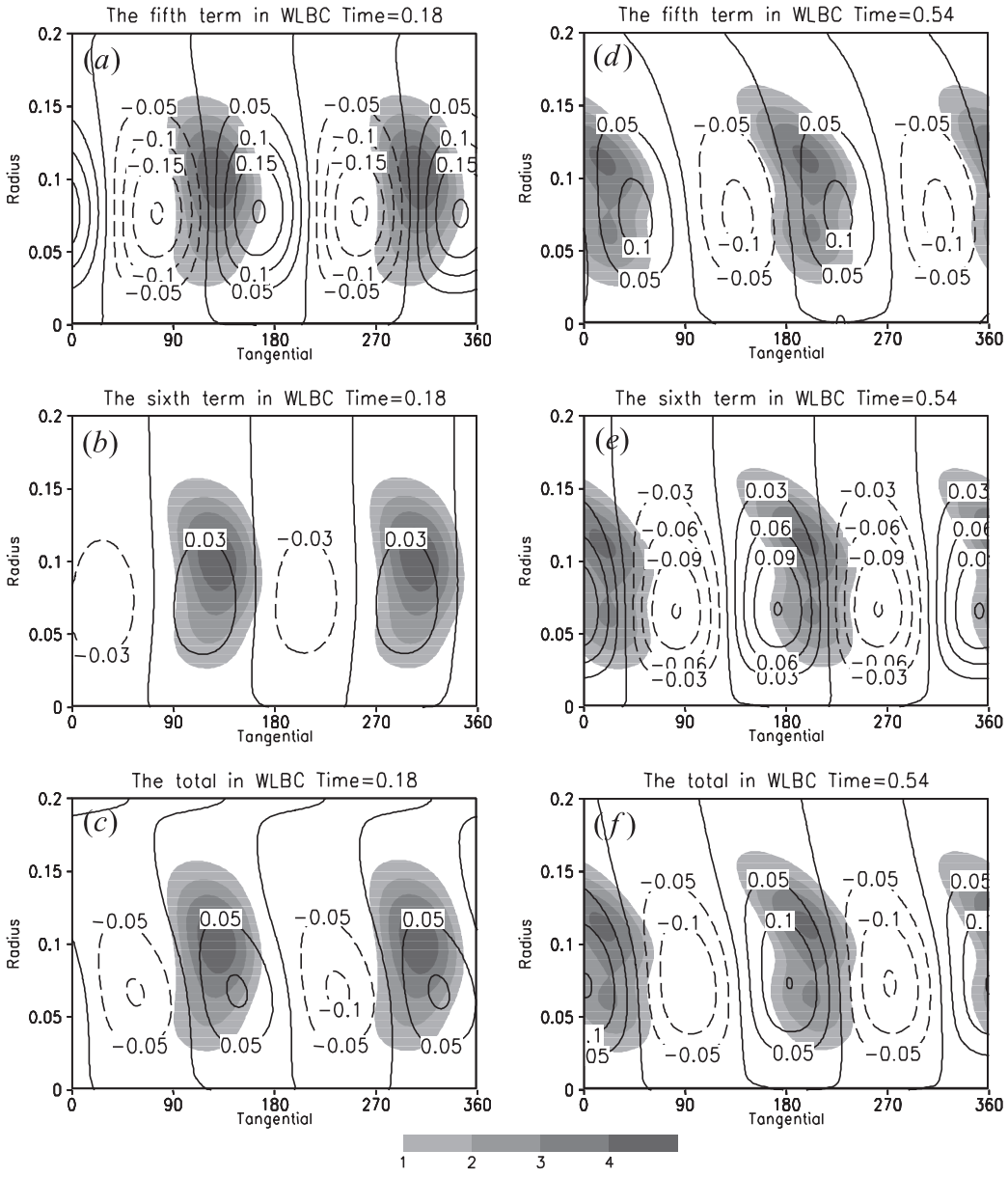

Fig. 3. The fifth term, sixth term, and the sum of terms on the right-hand side of the OMEGA equation in case WLBC at time (a, b, c) 0.18, (d, e, f) 0.54, (g, h, i) 0.72, and (j, k, l) 1.08. Shading represents the positive asymmetric vorticity.

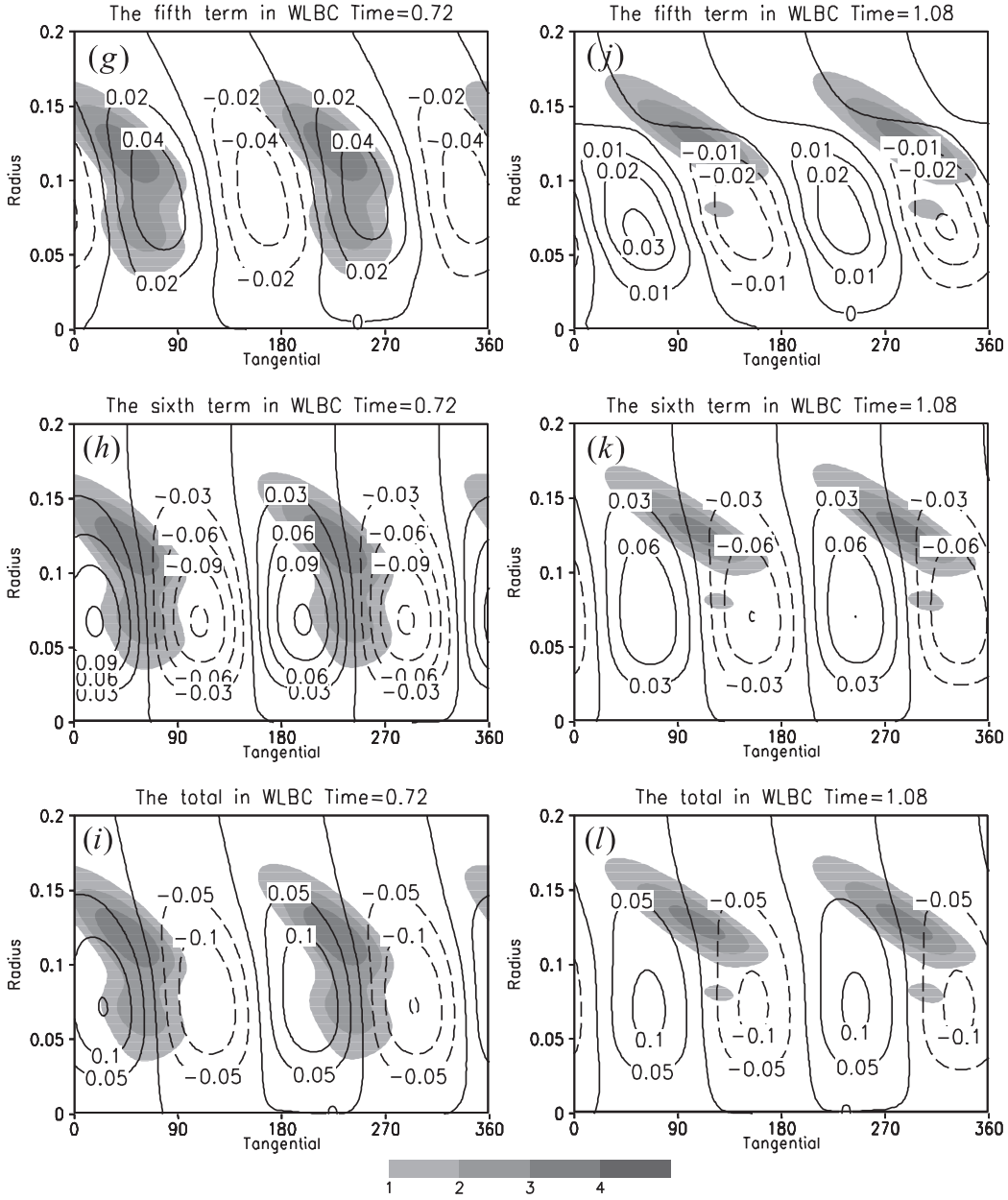

Fig. 3. (Continued).

and inside the RMW will generate upward motion ($\omega_2 < 0$) accompanied by convergence at the lower level ($\delta_3 < 0$) and divergence at the upper level before time 0.72 (Figs. 3a–i). The cold advection has more of an effect on the outer part of the asymmetric vorticity at the lower level after time 0.72 (Figs. 3j–l), which induces downward motion, divergence at the lower level and convergence at the upper level. Consequently, the warm (cold) advection by the barotropic mean (perturbation) flow in this case causes the phase difference between the lower-level asymmetric divergence and vorticity; therefore, the asymmetric divergence modifies the energy propagation of the vortex Rossby wave and makes the vortex axisymmetrization faster in the WLBC case than in the corresponding barotropic vortex case, LBC.

The baroclinic perturbations in the strong baroclinic vortex (SLBC) will generate a stronger lower-level asymmetric vorticity inside the RMW in the early stage (Fig. 1b) than in the weak baroclinic vortex (WLBC) (Fig. 1a) due to a stronger positive effect of the divergence on the lower-level asymmetric vorticity inside the RMW before time 0.72 (Figs. 4a–c). On the other hand, the stronger negative effect by the divergence is imposed on the asymmetric vorticity near the outer cell after time 0.72 (Fig. 4d), resulting in a faster decay of the asymmetric vorticity amplitude in SLBC than WLBC (Fig. 1). It is found that the sixth term (the warm/cold advection by the barotropic perturbation flows) and the eighth term in Eq. (7) of Peng et al. (2014) (the OMEGA equation) in the SLBC case cause the phase difference between

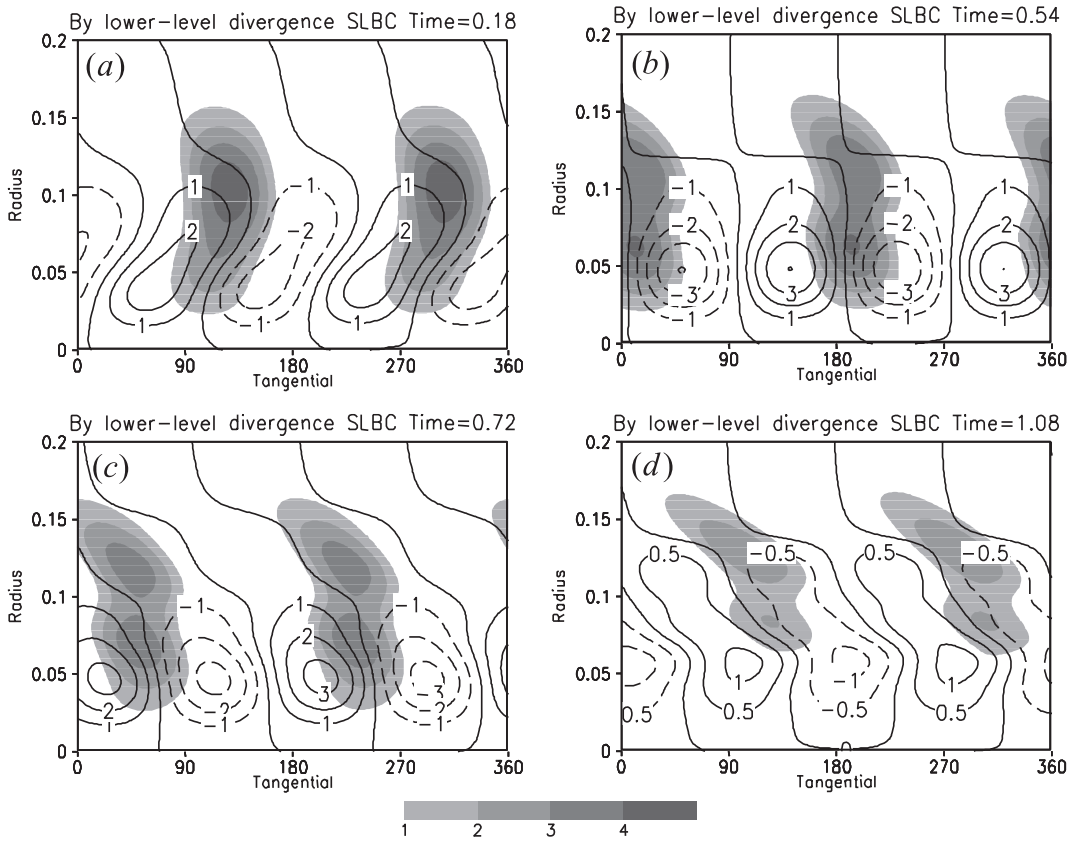

Fig. 4. The lower-level vorticity changed by divergence in case SLBC at time (a) 0.18, (b) 0.54, (c) 0.72, and (d) 1.08. Shading represents the positive asymmetric vorticity.

the lower level-asymmetric divergence and vorticity (figure not shown); therefore, the asymmetric divergence modifies the energy propagation of the vortex Rossby wave and makes the vortex axisymmetrization faster in SLBC case than the corresponding WLBC case.

2.2. *Nonlinear simulations*

Figure 7e in Peng et al. (2014), as well as Figs. 5a and d in the current paper, indicate that the nonlinear axisymmetrization process takes the longest time in a strong baroclinic vortex among the three different basic vortices. The comparison between the linear case, WLBC (Fig. 1a), and its corresponding nonlinear case, WNBC (Fig. 5a), indicates that the linear axisymmetrization process takes longer than in the nonlinear process. However, the linear axisymmetrization process by the stronger baroclinic vortex will take a shorter time than the corresponding nonlinear process (Fig. 1b vs. Fig. 5d).

The lower-level symmetric KE tendency is calculated in the following to delineate the nonlinear axisymmetrization. The lower-level symmetric KE tendency equation is

$$\frac{\partial \overline{K}_3}{\partial t} = \frac{\partial \overline{K}_a}{\partial t} + \frac{\partial \overline{K}_d}{\partial t} - \left(\frac{\partial \bar{u}_a \bar{u}_d}{\partial t} + \frac{\partial \bar{v}_a \bar{v}_d}{\partial t} \right), \qquad (2)$$

where $\overline{K}_3$ is the lower-level symmetric KE, $\overline{K}_a$ is the barotropic symmetric KE, and $\overline{K}_d$ is the baroclinic symmetric KE. The terms on the right-hand side of Eq. (2) are given in Peng et al. (2014, Appendix B).

In the NBC experiment, $\bar{u}_d = 0$, $\bar{v}_d = 0$, and $\overline{K}_d = 0$, so the symmetric KE at the lower level is equal to the barotropic symmetric KE ($\overline{K}_3 = \overline{K}_a$), while the tendency of the lower-level symmetric KE is the same as that of the barotropic symmetric KE, i.e., $\partial \overline{K}_3/\partial t = \partial \overline{K}_a/\partial t$. As the barotropic asymmetric KE is one order of magnitude smaller than the baroclinic asymmetric KE, the lower-level asymmetric KE in NBC is almost equal to the baroclinic asymmetric KE in experiment NBC. On the other hand, the barotropic symmetric KE in experiment SNBC is four orders of magnitude smaller than the corresponding baroclinic symmetric KE, i.e., $\overline{K}_a \approx 0$, so the tendency of the lower-level symmetric KE is the same as that of the baroclinic symmetric KE ($\partial \overline{K}_3/\partial t = \partial \overline{K}_d/\partial t$), and the symmetric KE at the lower level is equal to the baroclinic symmetric KE in experiment SNBC ($\overline{K}_3 = \overline{K}_d$).

The nonlinear axisymmetrization process takes longer in a stronger baroclinicity vortex due to the weaker KE transfer from asymmetric to symmetric circulations at the lower level [(Fig. 7d in Peng et al. (2014), and Figs. 5c and f in the current paper]. The energy transfer from asymmetric to symmetric flows is more efficient in the nonlinear case, WNBC, than in the linear case, WLBC, so the linear axisymmetrization process in WLBC takes longer than in the nonlinear axisymmetrization process in WNBC. On the other hand, less energy could be transferred from the asymmetric circulations to the symmetric flow, resulting in a slower nonlinear axisymmetrization in case SNBC than the corresponding linear pro-

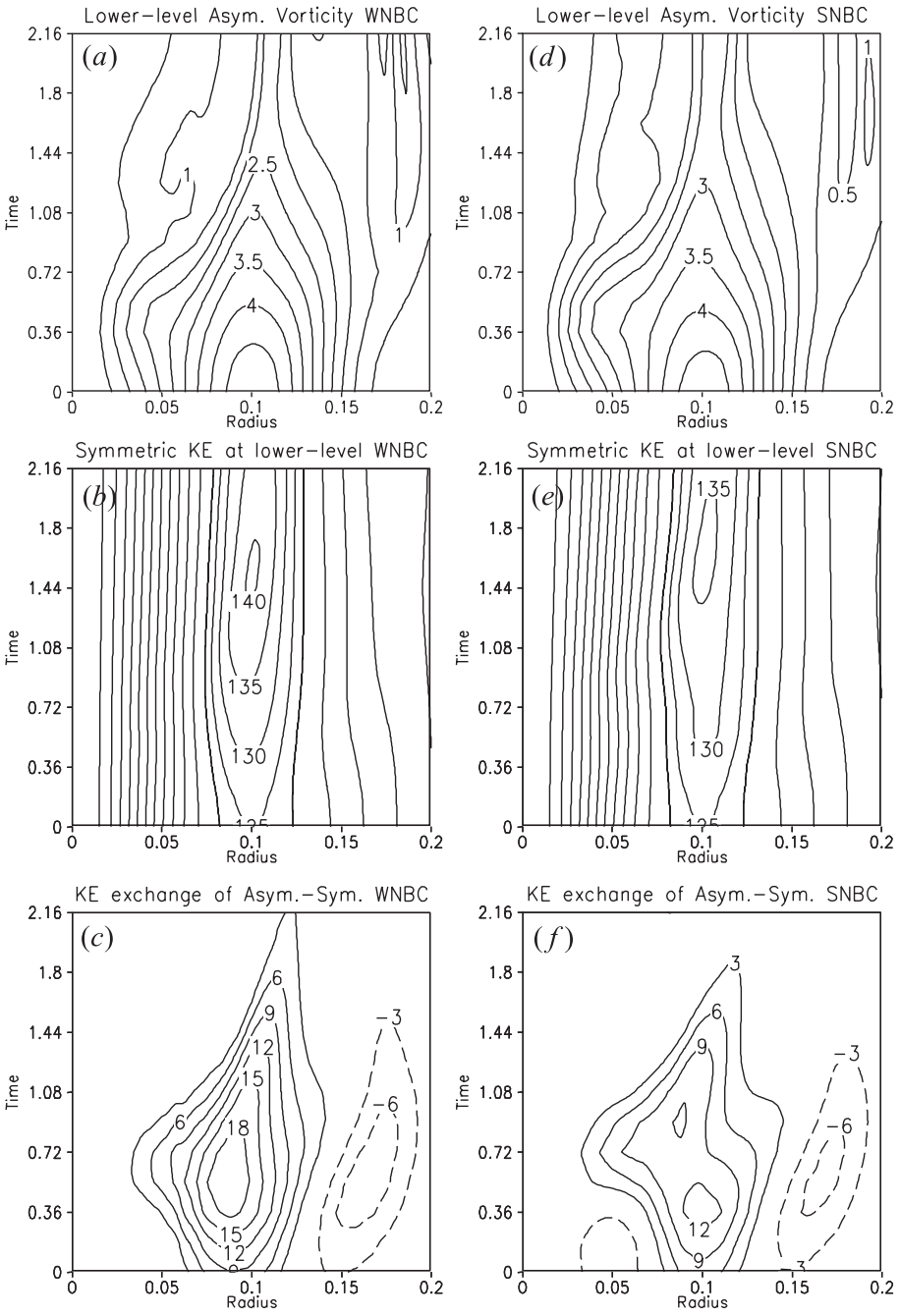

Fig. 5. The time–radius cross section of (a, d) asymmetric vorticity amplitude, (b, e) symmetric KE, and (c, f) the KE exchange between symmetric and asymmetric circulations at the lower level in case WNBC (left panels) and SNBC (right panels).

cess in case SLBC.

The symmetric vortex with a stronger baroclinicity is weaker at the lower level because less energy is gained from the asymmetric disturbances [Fig. 7b in Peng et al. (2014), and Figs. 5b and e in the current paper). The evolution of the maximum tangential wind in the nonlinear cases, NBC, WNBC and SNBC, is depicted in Fig. 6. The initial baroclinic asymmetric disturbances imposed near the RMW will intensify the lower-level basic state, with the largest increase in NBC, followed by WNBC, and the smallest in SNBC.

3. Energy conversion between barotropic and baroclinic components

In this section, we investigate the energy transferring among the four components, i.e., the barotropic (baroclinic) symmetric flows and asymmetric perturbations.

3.1. *Energy transfer in experiment SNBC*

In SNBC, initially, the lower-level positive vorticity centers are located at 90° and 270°, while the upper-level positive

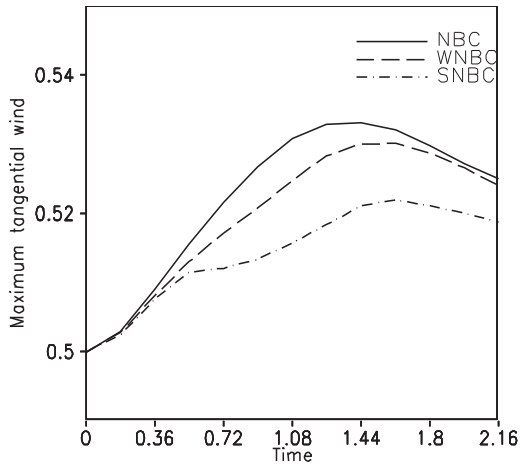

Fig. 6. The evolution of maximum tangential wind in the nonlinear cases (a) NBC (solid line), WNBC (dashed line), and SNBC (dashed–dotted line).

vorticity centers are located at 0° and 180°. Since the asymmetric vorticity centers at the upper and the lower level rotate in opposite directions by the symmetric flows, the vorticity centers at each level need to rotate 45° to become in phase. This occurs at around time 0.18. Once the asymmetric perturbations are in phase, they each need to rotate 90° in opposite directions in order for them to become out of phase. This occurs at around time 0.54. The asymmetric perturbations at the upper and lower levels are again in phase with each other at around time 0.72. In summary, the asymmetric perturbations have the stronger barotropic structure at time 0.18, 0.72, 1.26 and 1.8, and the stronger baroclinic structure at time 0.0, 0.54, 1.08, 1.62 and 2.16 (figure not shown).

The initial baroclinic asymmetric perturbations will generate the barotropic asymmetric perturbations by the baroclinic wave–mean flow interactions [the fourth term on the right-hand-side of Eq. (B3) in Peng et al. (2014, Appendix B)]. The barotropic asymmetric KE then increases to its maximum, while the initial baroclinic asymmetric KE decreases to a minimum at time 0.18 by the interactions of barotropic disturbance and baroclinic basic flow [the fourth term on the right-hand-side of Eq. (B4) in Peng et al. (2014, Appendix B)]. The evolution of the barotropic asymmetric KE is out of phase with that of the baroclinic asymmetric KE (figure omitted).

The baroclinic symmetric KE is four orders of magnitude greater than the corresponding barotropic symmetric KE (Fig. 7a), so the barotropic symmetric flow could be neglected in experiment SNBC. The interactions between the barotropic and baroclinic disturbances cause the energy transfer from asymmetric perturbation to the baroclinic symmetric flows [the third term on the right-hand-side of Eq. (B2) in Peng et al. (2014, Appendix B), and Fig. 7b in the present paper]. The baroclinic symmetric KE change rate at $r = 0.1$ indicates that the barotropic and baroclinic wave–wave interactions are the key dynamic processes, rather than the radial advection of baroclinic symmetric KE by the barotropic

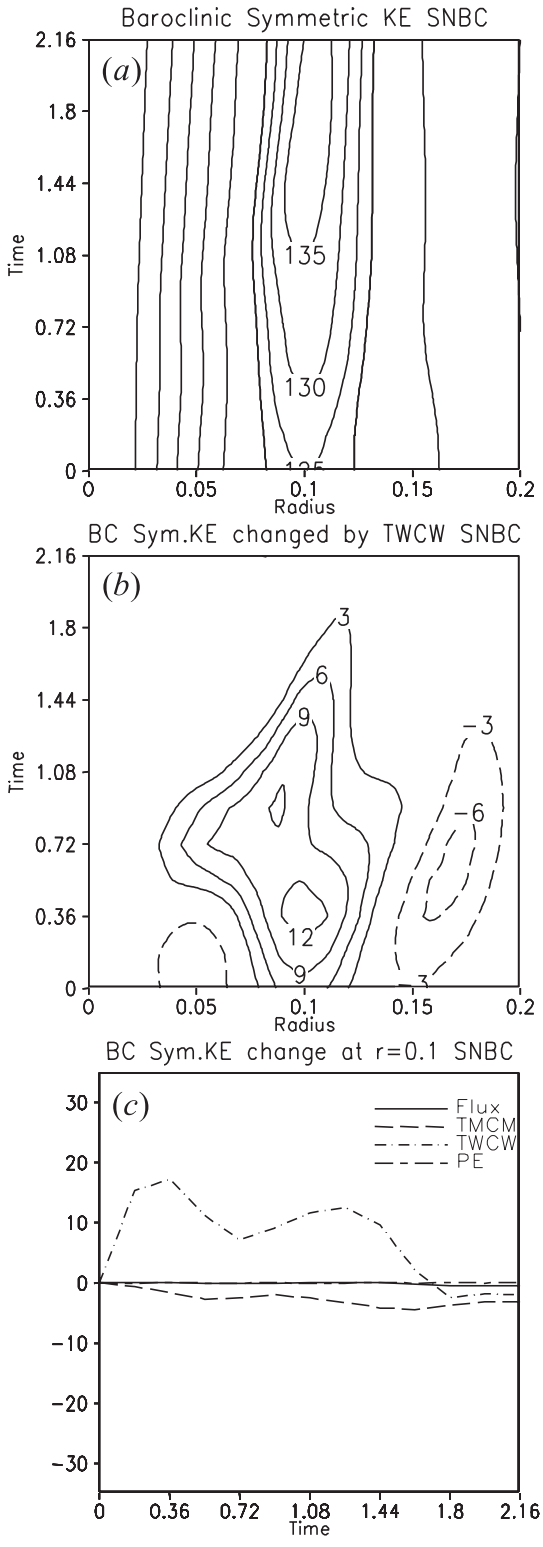

Fig. 7. The time–radius cross-section of (a) baroclinic symmetric KE and (b) its change rate by the interactions of barotropic and baroclinic waves. (c) The evolution of baroclinic symmetric KE change rate at $r = 0.1$ by the radial flux of baroclinic symmetric KE (solid line), by barotropic and baroclinic flow interactions (dashed line), by barotropic and baroclinic wave interactions (dashed–dotted line), and the radial advection of baroclinic potential energy (long–short line) in experiment SNBC.

symmetric flow, the interactions of barotropic and baroclinic flows, and the radial advection of the baroclinic symmetric potential energy (Fig. 7c).

There are three dominant terms in the interactions between the barotropic and baroclinic disturbances [the third term on the right-hand-side of Eq. (B2) in Peng et al. (2014, Appendix B)]. They are: $-\bar{v}_d\overline{u'_a v'_d}/r$, $-\bar{v}_d\overline{u'_d v'_a}/r$ and $-\bar{v}_d[\overline{u'_a(\partial v'_d/\partial r)} + \overline{u'_d(\partial v'_a/\partial r)}]$. Note that the baroclinic symmetric flows are always negative ($\bar{v}_d < 0$). At time 0.18, the barotropic asymmetric vorticity center is located upstream of the adjacent baroclinic asymmetric vorticity center, which induces $\overline{u'_a v'_d} > 0$ and $\overline{u'_d v'_a} < 0$ (figure omitted). Therefore, the baroclinic symmetric flows obtain energy from the asymmetric perturbations by $-\bar{v}_d\overline{u'_a v'_d}/r > 0$, and lose energy to the asymmetric perturbations by $-\bar{v}_d\overline{u'_d v'_a}/r < 0$ at the same time (figure omitted). The baroclinic tangential momentum advection by the barotropic radial perturbation flows and the barotropic tangential momentum advection by the baroclinic radial perturbation flows make the energy transfer from the asymmetric perturbation to symmetric flows near the RMW, which is the main contribution term (figure not shown). However, the barotropic asymmetric vorticity center shifts downstream of the adjacent baroclinic asymmetric vorticity center at time 0.36, which makes $\overline{u'_a v'_d} < 0$ and $\overline{u'_d v'_a} > 0$. Therefore, the asymmetric perturbations obtain energy from the baroclinic symmetric flows by $-\bar{v}_d\overline{u'_a v'_d}/r < 0$, while transferring their energy to the baroclinic symmetric flows by $-\bar{v}_d\overline{u'_d v'_a}/r > 0$ (figure omitted), exactly out of phase with the energy transfer at time 0.18. The most important energy transferring term is the momentum advection term that makes the energy conversion from the asymmetric perturbation to symmetric flows near the RMW (figure not shown). The energy conversion process at time 0.54 is the same as that at time 0.18, while the energy transfer process at time 0.72 is the same as that at time 0.36, and so on.

In summary, the initial baroclinic asymmetric perturbations in experiment SNBC can generate barotropic asymmetric perturbations through baroclinic wave–mean flow inter-

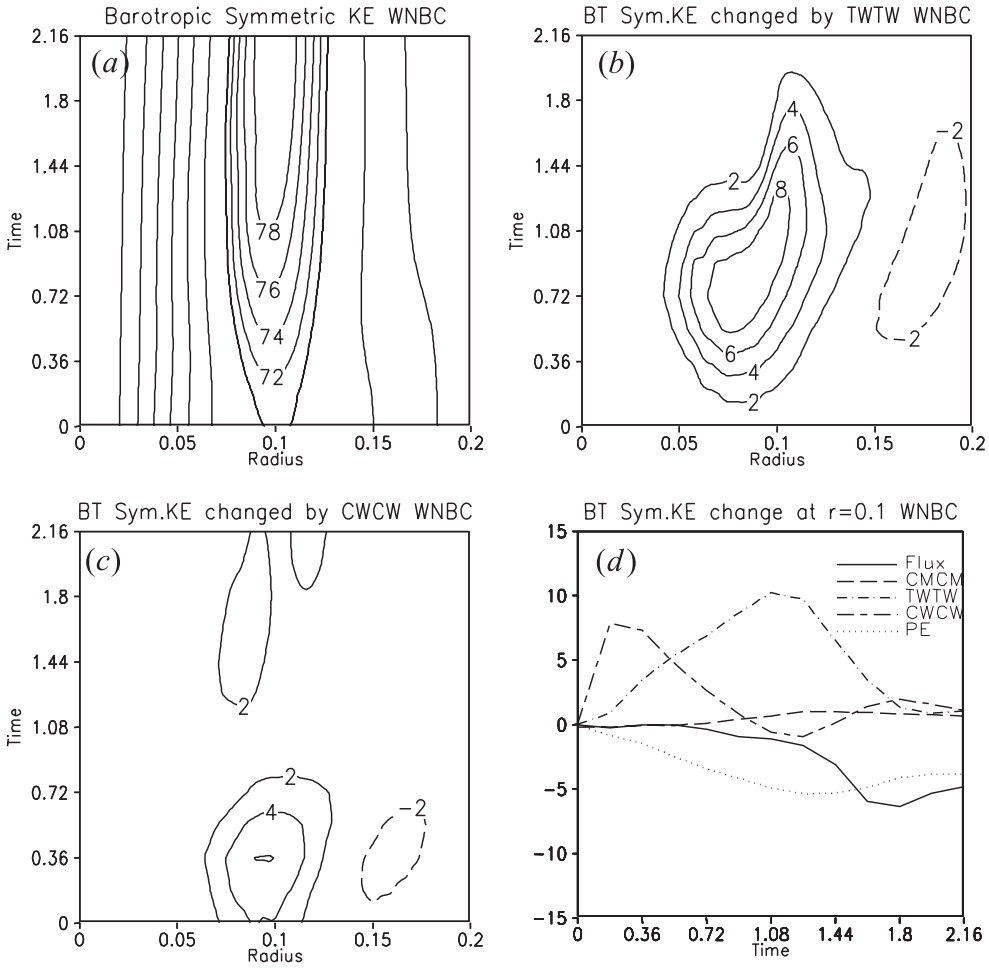

Fig. 8. The time–radius cross section of (a) barotropic symmetric KE and their change rate by (b) barotropic wave–wave and (c) baroclinic wave–wave interactions. (d) The evolution of barotropic symmetric KE change rate at $r = 0.1$ by radial flux of barotropic symmetric KE (solid line), baroclinic symmetric flow–flow interactions (dashed line), barotropic wave–wave interactions (dashed–dotted line), baroclinic wave–wave interactions (long–short line), and the radial advection of barotropic symmetric potential energy in experiment WNBC.

actions. Later, the barotropic asymmetric perturbations can feed the energy back to the baroclinic asymmetric perturbations by the interactions of barotropic disturbances and baroclinic flows. The baroclinic symmetric kinetic energy is changed by the barotropic and baroclinic wave interactions. The detailed energy conversion process in experiment SNBC is delineated in Fig. 10b.

3.2. *Energy transfer in experiment WNBC*

Observations indicate that the symmetric circulations of a tropical cyclone usually have a stronger barotropic component and a weaker baroclinic component (Marks and Houze, 1987; Reasor et al., 2000; Rogers et al., 2012). TC3 is a weak baroclinic tropical cyclone that contains a strong cyclonic flow ($\bar{V}_{\max} = 0.5$) at the lower level and a weak cyclonic flow ($\bar{V}_{\max} = 0.25$) at the upper level.

The initial baroclinic asymmetric perturbations in experiment WNBC will generate the barotropic asymmetric perturbations by the baroclinic wave–mean flow interactions [the fourth term on the right-hand-side of Eq. (B3) in Peng et al. (2014, Appendix B)]. The barotropic asymmetric KE then increases to a maximum at time 0.72, while the initial baroclinic asymmetric KE decreases to a minimum by the interactions of the barotropic wave and baroclinic flow [the fourth term on the right-hand-side of Eq. (B4) in Peng et al. (2014, Appendix B)]. Later, the barotropic asymmetric KE decreases while the baroclinic asymmetric KE increases slightly (figure omitted). Compared with experiment SNBC, the period of the energy conversion between the barotropic and baroclinic asymmetric circulations in experiment WNBC is larger, attributed to a smaller baroclinic symmetric flow in TC3 than in TC2.

The barotropic symmetric KE near $r = 0.1$ increases with time, which is due to energy transfer from the barotropic or baroclinic asymmetric perturbations to symmetric flows by the barotropic wave–wave interactions and the baroclinic wave–wave interactions (Figs. 8b and c). Due to the downshear tilt of the barotropic or baroclinic asymmetric vorticity structure, the barotropic or baroclinic momentum flux near $r = 0.1$ is positive ($-\overline{u'_a v'_a} > 0$ or $-\overline{u'_d v'_d} > 0$, figures omitted), and their gradient with r are positive ($-\partial\overline{(u'_a v'_a)}/\partial r > 0$ or $-\partial\overline{(u'_d v'_d)}/\partial r > 0$), which causes the energy transfer from asymmetric perturbations to symmetric flows. It is interesting to note that the barotropic symmetric KE change rate at $r = 0.1$ by the barotropic wave–wave interactions is out of phase with that by the baroclinic wave–wave interactions. The other three terms (the first, second and fifth term) on the right-hand-side of Eq. (B1) (Peng et al., 2014, Appendix B) have fewer effects on the evolution of the barotropic symmetric KE (Fig. 8d).

The baroclinic symmetric KE change rate is less than that of the barotropic symmetric KE in experiment WNBC, because the interactions between the barotropic and baroclinic waves makes a smaller energy transfer from the asymmetric perturbation to symmetric flows [the third term on the right-hand side of Eq. (B2) in Peng et al. (2014, Appendix B),

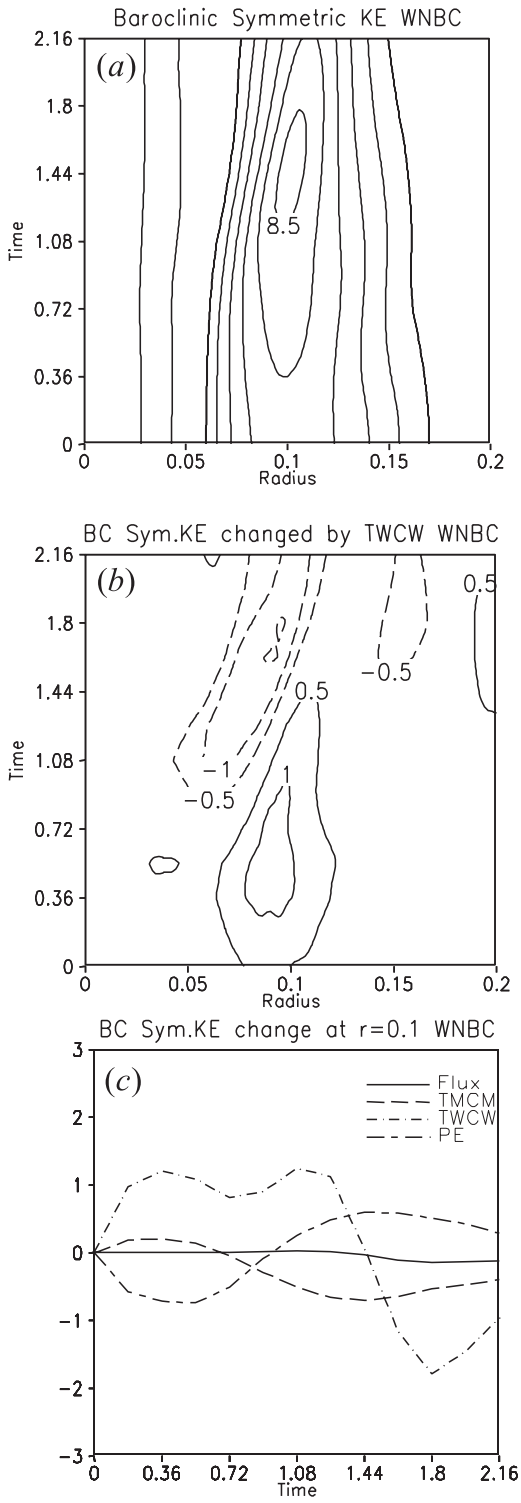

Fig. 9. The time–radius cross section of (a) baroclinic symmetric KE and their change rate by (b) the interactions of barotropic and baroclinic waves. (c) The evolution of baroclinic symmetric KE change rate by radial flux of baroclinic symmetric KE (solid line), barotropic and baroclinic mean flow interactions (dashed line), barotropic and baroclinic wave interactions (dashed–dotted line), and the radial advection of baroclinic symmetric potential energy (long–short line) in experiment WNBC.

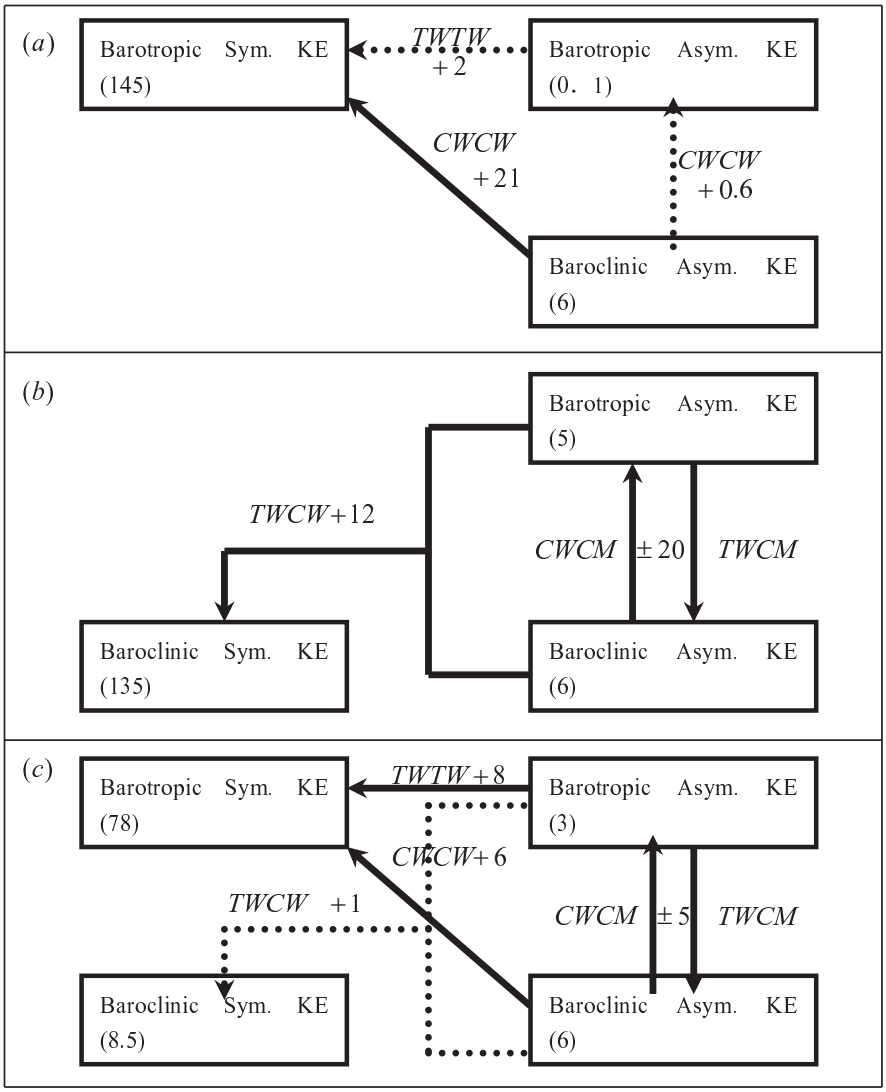

Fig. 10. The energy transfer diagrams in experiment (a) NBC, (b) SNBC and (c) WNBC. TWTW and CWCW indicate the barotropic wave–wave interactions and the baroclinic wave–wave interactions. TWCW, CWCM and TWCM indicate the interactions of barotropic and baroclinic waves, the interactions of the baroclinic wave and baroclinic mean flow, and the interactions of the barotropic wave and baroclinic mean flow. The solid (dotted) arrows indicate a strong (weak) energy conversion rate.

and Fig. 9b in the present paper]. The baroclinic symmetric KE change rate at $r = 0.1$ indicates that the barotropic and baroclinic wave interactions are stronger than the other three terms on the right-hand side of Eq. (B2) (Peng et al., 2014, Appendix B) (Fig. 9c). Similar to experiment SNBC, the barotropic asymmetric vorticity center is located upstream of the adjacent baroclinic asymmetric vorticity center at time 0.36 and 0.72 (figure not shown), which makes the energy transfer from asymmetric perturbations to baroclinic symmetric flows in terms of $-\bar{v}_{\rm d}\overline{u'_{\rm a}v'_{\rm d}}/r > 0$, while energy of the baroclinic symmetric flows lose to asymmetric perturbations in terms of $-\bar{v}_{\rm d}\overline{u'_{\rm d}v'_{\rm a}}/r < 0$ (figure omitted). However, the barotropic asymmetric vorticity center shifts downstream of the adjacent baroclinic asymmetric vorticity center at time 1.08 and 1.44. Therefore, the asymmetric perturbations obtain energy from the baroclinic symmetric flows by $-\bar{v}_{\rm d}\overline{u'_{\rm a}v'_{\rm d}}/r < 0$, while transferring their energy to the baroclinic symmetric flows by $-\bar{v}_{\rm d}\overline{u'_{\rm d}v'_{\rm a}}/r > 0$ (figure omitted). The most important energy transfer term is the momentum advection term, which makes the energy conversion from the asymmetric perturbation to symmetric flows near the RMW (Fig. 9).

The major energy conversion process for experiment WNBC is shown in Fig. 10c. The barotropic and baroclinic asymmetric perturbations could exchange their energy with each other through baroclinic wave–mean flow interactions, as well as barotropic wave and baroclinic mean flow interactions. The barotropic or baroclinic wave–wave interac-

tions have the greater effect on the energy change of the barotropic symmetric flows, while the interactions between the barotropic and baroclinic waves have less effect on the energy evolution of the baroclinic symmetric flows.

4. Summary and discussion

This paper investigates the axisymmetrization process of baroclinic disturbances by vortices with different baroclinicity on the basis of a two-layer dynamic model. The study focuses on energy exchange among different components.

A stronger inner-core asymmetry can be generated in a stronger baroclinic vortex with the same initial baroclinic perturbations. The radial propagation of the vortex Rossby wave at the lower level is faster in the stronger baroclinic vortex, resulting in a faster axisymmetrization for the same initial baroclinic perturbations. Therefore, the stronger baroclinic vortex gains less energy from the asymmetric disturbances resulting in a weak cyclonic circulation at the lower level.

The baroclinic wave–wave interactions can cause large energy transfer to the barotropic vortex due to the downshear tilt of baroclinic asymmetric vorticity perturbations near the RMW. In the strong baroclinic vortex, the initial baroclinic perturbations can generate the barotropic perturbations. The barotropic and baroclinic asymmetric KEs are interchanged due to the different basic flows at each level, making the growth and decay of barotropic and baroclinic asymmetric perturbations out of phase. Furthermore, the nonlinear interactions of the barotropic and baroclinic waves intensify the baroclinic symmetric vortex near the eyewall region due to the phase difference between the barotropic and baroclinic asymmetric vorticity disturbances.

The barotropic asymmetry in the weak baroclinic vortex can be generated by the interactions between the baroclinic symmetric flows and the initial baroclinic asymmetric perturbations. The period of energy conversion between the barotropic and baroclinic asymmetric perturbations is larger than that in the strong baroclinic vortex, which is attributed to the smaller baroclinic symmetric flows in the weak baroclinic vortex. Both the barotropic and the baroclinic wave–wave interactions can intensify the barotropic symmetric circulations, while less intensification of the baroclinic symmetric flows is being induced by the interactions of barotropic and baroclinic disturbance.

The major finding of this study is that the same initial asymmetric perturbation can have different effects on symmetric vortices with different baroclinicity. In numerical weather prediction models, a synthetic vortex is usually added in the initial field to represent a TC without in situ data. This study implies that the vertical structure of the initial vortex can have a large influence on the simulated tropical cyclone intensity change in the later stages.

Acknowledgements. This work was supported by ONR Grants N000140310739 and PE 0602435N. The International Pacific Research Center is partially sponsored by the Japan Agency for Marine-Earth Science and Technology (JAMSTEC).

REFERENCES

Carr, L. E., and R. T. Williams, 1989: Barotropic vortex stability to perturbations from axisymmetry. *J. Atmos. Sci.*, **46**, 3177–3191.

Enagonio, J., and M. T. Montgomery, 2001: Tropical cyclogenesis via convectively forced vortex Rossby waves in a shallow water primitive equation model. *J. Atmos. Sci.*, **58**, 685–705.

Marks, F. D. Jr., and R. A. Houze Jr., 1987: Inner core structure of Hurricane Alicia from airborne Doppler radar observations. *J. Atmos. Sci.*, **44**, 1296–1317.

Möller, J. D., and M. T. Montgomery, 1999: Vortex Rossby-waves and their influence on hurricane intensification in a barotropic model. *J. Atmos. Sci.*, **56**, 1674–1687.

Möller, J. D., and M. T. Montgomery, 2000: Tropical cyclone evolution via potential vorticity anomalies in a three-dimensional balance model. *J. Atmos. Sci.*, **57**, 3366–3387.

Montgomery, M. T., and R. J. Kallenbanch, 1997: A theory for vortex Rossby-waves and its application to spiral bands and intensity changes in hurricanes. *Quart. J. Roy. Meteor. Soc.*, **123**, 435–465.

Montgomery, M. T., and J. Enagonio, 1998: Tropical cyclogenesis via convectively forced vortex Rossby wave in a three-dimensional quasi-geostrophic model. *J. Atmos. Sci.*, **55**, 3176–3207.

Peng, J., M. S. Peng, and T. Li, 2008: Dependence of vortex axisymmetrization on the characteristics of the asymmetry. *Quart. J. Roy. Meteor. Soc.*, **134**, 1253–1268.

Peng, M. S., J. Peng, T. Li, and E. Hendricks, 2014: Effect of baroclinicity on vortex axisymmetrization. Part I: Barotropic basic vortex. *Adv. Atmos. Sci.*, **31**(6), doi: 10.1007/s00376-014-3237-x.

Reasor, P. D., M. T. Montgomery, F. D. Marks Jr., and J. F. Gamache, 2000: Low-wavenumber structure and evolution of the hurricane inner core observed by airborne dual-Doppler radar. *Mon. Wea. Rev.*, **128**, 1653–1680.

Rogers, R., S. Lorsolo, P. Reasor, J. Gamache, and F. D. Marks, 2012: Multiscale analysis of tropical cyclone kinematic structure from airborne Doppler radar composites. *Mon. Wea. Rev.*, **140**, 77–99.

Shapiro, L. J., 2000: Potential vorticity asymmetries and tropical cyclone evolution in a moist three-layer model. *J. Atmos. Sci.*, **57**, 3645–3662.

Smith, G. B. II, and M. T. Montgomery, 1995: Vortex axisymmetrization: Dependence on azimuthal wavenumber or asymmetric radial structure changes. *Quart. J. Roy. Meteor. Soc.*, **121**, 1615–1650.

Wang, Y., 2002: Vortex Rossby waves in a numerically simulated tropical cyclone. Part 1: Overall structure, potential vorticity and kinetic budgets. *J. Atmos. Sci.*, **59**, 1213–1238.